

## Article

# Sea-Surface Characteristics of the Newfoundland Basin of the Northwest Atlantic Ocean during the Last 145,000 Years: A Study Based on the Sedimentological and Paleontological Proxies

Harunur Rashid <sup>1,2,\*</sup> , Qian Qian Lu <sup>1</sup>, Min Zeng <sup>1</sup>, Yang Wang <sup>1</sup> and Zhao Wu Zhang <sup>1</sup>

- <sup>1</sup> College of Marine Sciences, Shanghai Ocean University, Shanghai 201306, China; m180200468@st.shou.edu.cn (Q.Q.L.); d200200045@st.shou.edu.cn (M.Z.); m180200479@st.shou.edu.cn (Y.W.); m200200653@st.shou.edu.cn (Z.W.Z.)
- <sup>2</sup> Earth and Environmental Sciences, Memorial University of Newfoundland, Corner Brook, NL A2H 6P9, Canada
- \* Correspondence: Harunurbhola@gmail.com



**Citation:** Rashid, H.; Lu, Q.Q.; Zeng, M.; Wang, Y.; Zhang, Z.W. Sea-Surface Characteristics of the Newfoundland Basin of the Northwest Atlantic Ocean during the Last 145,000 Years: A Study Based on the Sedimentological and Paleontological Proxies. *Appl. Sci.* **2021**, *11*, 3343. <https://doi.org/10.3390/app11083343>

Academic Editor: Valeria Luciani

Received: 14 January 2021

Accepted: 11 March 2021

Published: 8 April 2021

**Publisher's Note:** MDPI stays neutral with regard to jurisdictional claims in published maps and institutional affiliations.



**Copyright:** © 2021 by the authors. Licensee MDPI, Basel, Switzerland. This article is an open access article distributed under the terms and conditions of the Creative Commons Attribution (CC BY) license (<https://creativecommons.org/licenses/by/4.0/>).

**Abstract:** Dramatic changes occur in the sea-surface characteristics (i.e., temperature and salinity) and freshwater input due to the interaction of cold and fresh Labrador Current and warm and salty North Atlantic Current (NAC) on the southeast Grand Banks. As a result, the biological productivity and seasonal stratification of the upper water masses are intensified. Such changes must have been more dramatic during the glacial times due to the penetration of the Polar and Arctic fronts and southward migration of the Gulf Stream/NAC. However, the extent to which such changes impacted the sea-surface characteristics in the Newfoundland Basin is poorly known. We report changes in the sea-surface characteristics using a piston core (Hu9007-08) collected from the Milne seamount during the last 145,000 years. Heinrich layers H1, H2, H4, and H5 and H11 within the MIS3 and at the penultimate deglaciation were identified by the ice-rafted detritus (IRD) and *Neogloboquadrina pachyderma* peaks and lighter oxygen isotopes. Rapid turnover by the foraminiferal species with distinct depth habitats and ecological niches in the mixed-layer and thermocline suggests an interplay between the polar and subpolar water masses during the Heinrich and non-Heinrich periods. Only two North Atlantic-wide cooling events, C24 and C21, in which the latter event linked to the minor IRD event during the marine isotope stage (MIS) 5 in Hu90-08, compared to the eight events in the eastern subpolar gyre (e.g., ODP site 984). Millennial-scale *N. pachyderma* variability in the western subpolar gyre appears to be absent in the eastern subpolar gyre during the MIS3 suggesting the occasional presence of salty and warm water by the NAC inflow, implying a different climate state between the western and eastern subpolar gyre. Although *T. quinqueloba* data are fragmentary, there are differences between the western and eastern subpolar gyre in addition to the differences within the western subpolar gyre during MIS5 that might imply a variable influence by the subpolar water. This finding suggests that the influence by the NAC outweighs the impact of cold and fresh polar water in the northern northwest Atlantic during the MIS5.

**Keywords:** Heinrich events; foraminiferal assemblages; Labrador Current; marine isotope stages; Newfoundland Basin

## 1. Introduction

Due to the periodic expansions and contractions of the Laurentide Ice Sheet (LIS) during the last glacial cycle, enormous amounts of icebergs, sediments, and meltwater were discharged to the neighboring Labrador Sea and the North Atlantic [1]. These discharge events, known as the Heinrich events (H-events), are recorded as ice-rafted detritus (IRD) layers in the northwest Labrador Sea [2,3] and open North Atlantic [4,5], were the extreme manifestation of cold, abrupt climate events [6–8]. Employing a suite of sedimentological

and geochemical proxies (i.e., geomagnetic paleointensity, natural magnetization,  $\text{CaCO}_3$ , and oxygen isotopes ( $\delta^{18}\text{O}$ )) from a southwest Labrador Sea giant sediment core MD95-2024, Stoner et al. [9] identified H1 to H5 as detrital carbonate layers without reporting their impact on the sea-surface. Hiscott et al. [10] reported sea-surface temperatures (SSTs) applying the planktonic foraminiferal assemblages for the last 340,000 years from the nearby of core MD95-2024. However, the authors did not report foraminiferal census data, and hence, the impact of meltwater on the foraminiferal assemblages is unknown. Using a suite of sedimentological (Ca/Sr,  $\delta^{18}\text{O}$ , and  $>106\ \mu\text{m}$ ) and paleomagnetic proxies from the Integrated Ocean Drilling Program sites U1302/03, nearby the site MD95-2024, Channel et al. [11] reported the dynamics of the LIS during the last 720,000 years. Again, the foraminiferal assemblages data linked to Heinrich or other high-frequency IRD events are lacking, thus preventing assessing perturbation in the surface water properties. In short, the existing Labrador Sea records lack the integrated foraminiferal census data with  $\delta^{18}\text{O}$  to assess the impact of abrupt ice-rafting events.

Past H-events or abrupt Dansgaard-Oeschger (D/O) climate events' studies mainly report changes in the subtropical gyre or the expanded subpolar gyre during the glacial periods [5,12–15]. For example, Bond et al. [5,16] reported millennial-scale D/O cycles or H-events for marine isotope stage 3 (MIS3) using sediments from the Deep-Sea Drilling Program site 609 from the IRD-belt [17], currently located between subpolar and subtropical transitional zone (Figure 1). A few notable studies from the eastern subpolar gyre, namely Oppo and Lehman [18], Elliot et al. [19], Hodell et al. [20], Dokken et al. [21], and Barker et al. [22], also characterized changes in the sea-surface characteristics combining the usage of foraminiferal assemblages,  $\delta^{18}\text{O}$ , and sediment geochemistry. However, records from the western subpolar gyre are scarce except for Labeyrie et al. [23], in which core CH69-K09 from the foot of the Newfoundland Slope was used. The authors used foraminiferal assemblages,  $\delta^{18}\text{O}$ , and IRD count to report changes in the sea-surface conditions from MIS1 to MIS3, lacking records for the full last glacial cycle. Therefore, this study was conceived to document changes in the sea-surface characteristics from the Newfoundland Basin that resides in the western subpolar gyre for the last glacial cycle. The objectives of the study are to (a) obtain foraminiferal assemblages and concomitant IRD data to link to the Heinrich- and D/O events; (b) determine the  $\delta^{18}\text{O}$  in planktonic foraminifera to assess the impact of freshwater from the Heinrich- and D/O events; (c) construct the stratigraphy using the  $^{14}\text{C}$ -AMS dates and the  $\delta^{18}\text{O}$ , and (d) employ data from this study in other suitable published data from the wider subpolar North Atlantic. In that context, data from cores CH69-K09 [23], EW9303-37JPC (hereafter 37JPC; [24]), and MD03-2664 [25,26] from the western subpolar gyre and SU90-24 [19] and the Ocean Drilling Program (ODP) site 984 [27] from the eastern gyre fit the purpose of this study. By doing so, the study will assess the impact of meltwater from the Heinrich- and D/O-ice rafting events on the planktonic foraminiferal assemblages and the interaction between the cold and fresh Labrador Current and warm and salty Gulf Stream/North Atlantic Current during the last glacial cycle. Further, the study will compare (1) changes in the mixed-layer and thermocline characteristics during the cold MIS2-3 and warm MIS5; and (2) assess similarities and dissimilarities between the western and eastern North Atlantic subpolar gyre.

## 2. Oceanographic Setting

The Newfoundland Basin lies on the southeastern Grand Banks of the Northwest Atlantic Ocean (Figure 1), a key area where the exchange between subpolar and subtropical gyres takes place. The Labrador Current brings southward flowing cold and freshwater, which is seasonally replaced by northward-flowing warm and salty water of the North Atlantic Current (NAC). These two powerful surface currents traverse on the west and east side of the Newfoundland Basin. The spatial interplay of these currents determines the SST and sea-surface salinity of the Basin. The Labrador Current is the continuation of the Western Greenland and Baffin Island currents, with average annual flow speeds of 25–35 cm/s [28]. The cold Labrador Current sweeps the entire northwest Atlantic continen-

tal margin (Figure 1) [1,29]). In contrast, the NAC is the continuation of the Gulf Stream (e.g., [30]) that flows through the Newfoundland Basin and transports warm and salty water to the northeast Atlantic, typically the strongest between 42° and 39.5° W [31]. At the southeastern tip of the Grand Banks of Newfoundland, part of the NAC recirculates or continues in an eastward direction, while the remaining fraction turns northward. It is also a critical region where the modern Labrador Current and NAC frequently interact.

The SST and salinity of the Northwest Atlantic Ocean, particularly in the Newfoundland Basin, greatly vary. The annual SSTs vary between 7° and 17.5 °C in the Newfoundland Basin. When the influence of the cold Labrador Current increases, the impact on the southeast Grand Banks of the northwestern edge of the Newfoundland Basin expands, and the SSTs significantly decrease (Figure 1). Conversely, when the influence of the warm and salty NAC increases, the SSTs on the southeastern edge of the Newfoundland Basin increase resulting in a decrease in temperatures between the eastern and western sides of the Basin. It can be seen that the sea-surface of the Newfoundland Basin is mainly affected by the warm and salty NAC in the summer, and the cold Labrador Current has a smaller range. Down-depth SST plot (Figure 2b) suggests that the temperature rapidly decreases to 7 °C at ~500 m in the west, whereas the 7 °C isotherm crops out on the southeastern Grand Banks reflecting the spatial extent of the Labrador Current. The spatial impact of the Labrador Current and North Atlantic Current is also demonstrated by the salinity gradient (Figure 2c) between the eastern and western Newfoundland Basin.

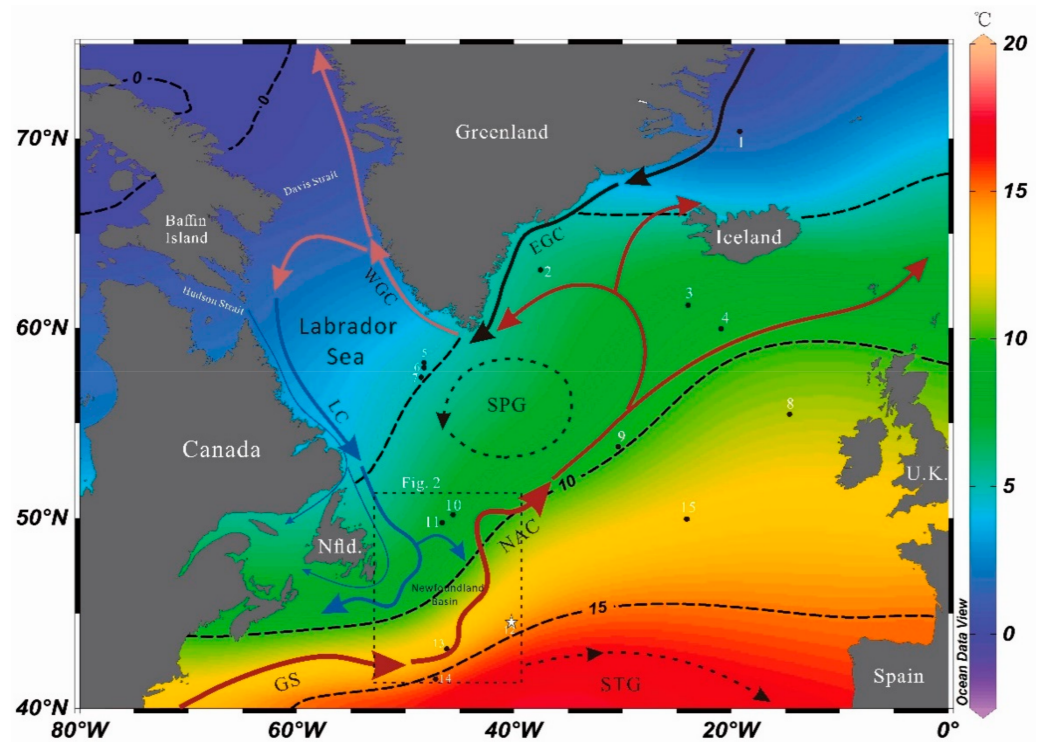


**Figure 1.** General oceanographic features of the modern northwest Atlantic Ocean. The mean annual sea-surface temperature with 5 °C contour demarcates between the subpolar and subtropical gyres. The location of the cores used in this study is listed in Table 1. Note that “white star” denotes the location of core Hu90-08 (this study). The tabular box with the discontinuous line shows the location of Figure 2. GS = Gulf Stream; NAC = North Atlantic Current; EGC = East Greenland Current; WGC = West Greenland Current; LC = Labrador Current; SPG = Subpolar gyre; and STG = Subtropical gyre.

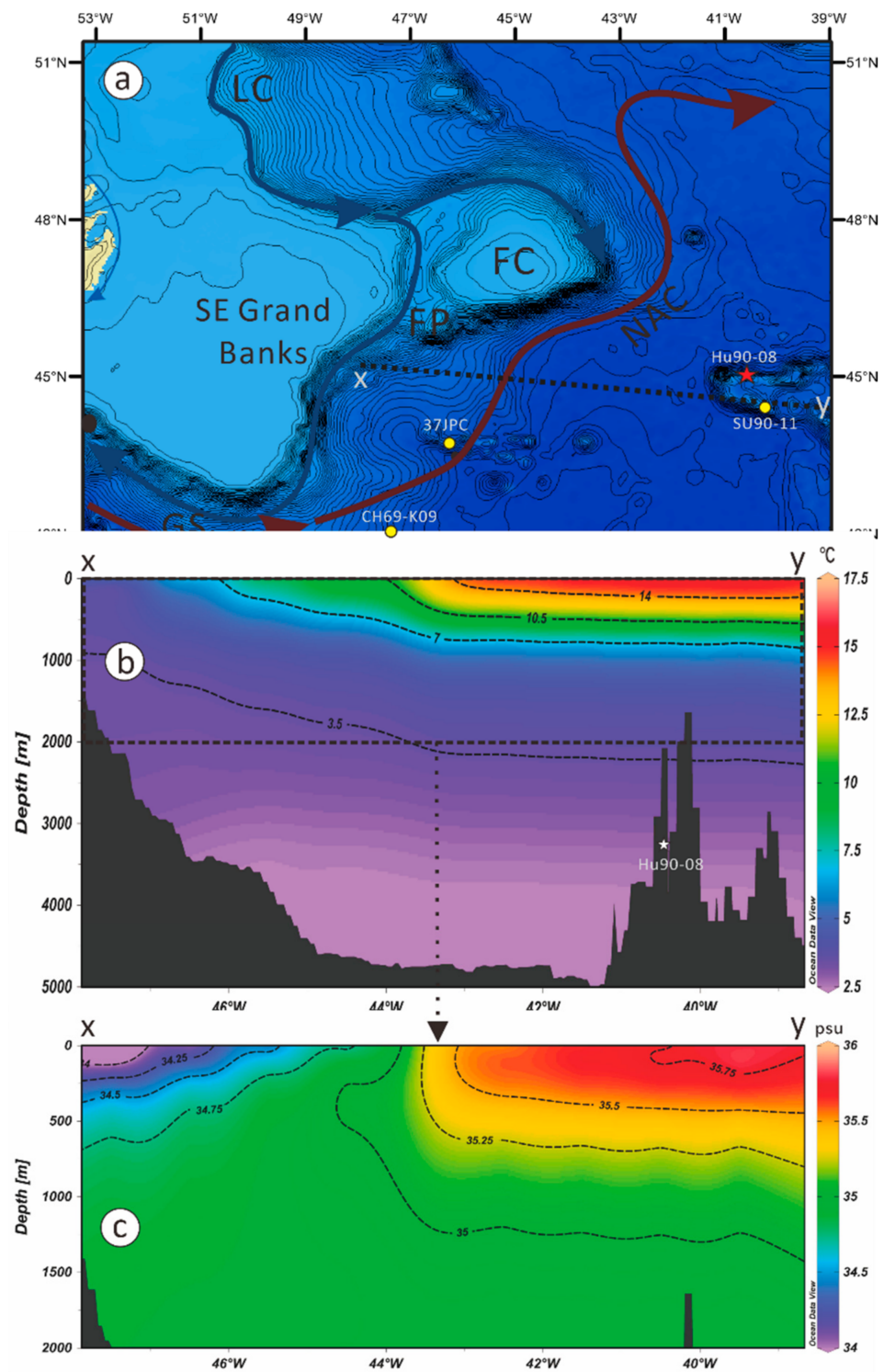


**Figure 2.** (a) enlarged bathymetric map of the SE Grand Banks, SW Labrador Sea, and Newfoundland Basin. The location of the published records of a few cores used in the study is shown by the yellow dots, whereas the position of the sediment core Hu9007-08 (this study) is shown by the red star. (b) sea-surface temperature distribution on the SE Grand Banks on the X-Y transect is shown in Figure 2a. (c) sea-surface salinity along the X-Y section, which demonstrates the low salinity Labrador Current (west), whereas the position of the North Atlantic Current is shown by the high salinity (east). Note LC = Labrador Current; GS = Gulf Stream; NAC = North Atlantic Current; FC = Flemish Cap; and FP = Flemish Pass. Figure 2b,c were plotted using the Ocean Data View software [32].

### 3. Materials and Methods

#### 3.1. Sediment Samples

The core Hu9007-08 (hereafter Hu90-08; 44.5329° N and 40.3855° W) was retrieved at 3522 m water depth top of Milne seamount from the eastern Newfoundland Basin of the northwest Atlantic Ocean by the joint Memorial University of Newfoundland and Geological Survey of Canada cruise. The core site is located near the western edge of the IRD-belt (Figure 1), too far from the eastern Canadian continental margin to be influenced by the mass-transport deposits [1]. Therefore, the core site is an ideal location to study past changes in the sea-surface conditions. Core Hu90-08 is 11 m long, but the top 841.5 cm was used for this study, which was sampled at 10 cm intervals. However, the MIS3 period was sampled at 5 cm intervals to improve the temporal resolution (i.e., 400 to 1000 years).

**Table 1.** Location of cores used in the study.

	Core ID	Latitude (N)	Longitudes (W)	Water Depth (m)	Reference
1	M23351	70.35°	18.2167°	1673	Zhuravleva et al. [33]
2	SU90-24	63.1167°	37.6305°	2085	Elliot et al. [19]
3	ODP 984	61.25°	24.04°	1648	Mokeddem et al. [27]
4	V29-202	60°	21°	2658	Oppo and Lehman [18]
5	Hu90013-013	58.2167°	48.3667°	3380	Hillaire-Marcel et al. [34]
6	MD99-2227	58.2°	48.3667°	3460	Carlson et al. [35]
7	MD03-2664	57.439°	48.6058°	3442	Irvali et al. [25]
8	ODP 980	52.29°	14.42°	2179	Oppo et al. [36]
9	NEAP18K	53.7667°	30.35°	3175	Chapman & Shackleton [37]
10	Hu91045-094	50.2043°	45.6857°	3448	de Vernal et al. [38]
10	MD95-2024	50.1226°	45.4114°	3448	Stoner et al. [9]
11	MD95-2025	49.7941°	46.6975°	2925	Hiscott et al. [10]
12	Hu9007-08	44.5329°	40.3855°	3522	This study
13	EW9303-37JPC	43.1°	46.0333°	3981	McManus et al. [24]
14	CH69-K09	41.7567°	47.35°	4100	Labeyrie et al. [23]
15	DSDP 609	49.8833°	24.2333°	3884	Rashid and Boyle [39] Bond et al. [5]

#### 3.2. Sediment Processing

##### 3.2.1. Sample Washing

Sediments were freeze-dried, weighed, and soaked in deionized water for 24 h to disperse. Samples were then ultrasonicated (up to 5 s) while stirring, then rinsed through a 63 µm diameter sieve. The washed residues were dried using an oven at 60 °C and stored in glass vials. Sediments <63 µm were allowed to stand for 24 h, and the supernatant was poured out and dried, and stored for future analysis.

##### 3.2.2. IRD and Planktonic Foraminifer Count

The >63 µm fractions were sieved again with a 150 µm sieve and weighed and were used to identify and count planktonic foraminifera and IRD. Each sample was divided equally about 7–9 times by a splitter when the total number of planktonic foraminifer complete shells is within the range of 300–600. Using a micropaleontological tray, foraminifers were identified and counted, and IRD was also counted [5,40]. After completing foraminiferal assemblages count, the statistical treatment such as absolute abundance, percentage of each species, trends, etc., was carried out.

##### 3.2.3. Oxygen and Carbon Isotopes Determination

Five to 10 clean and unstained *N. pachyderma* in the 150–250 µm size fractions were used to determine  $\delta^{18}\text{O}$  and  $\delta^{13}\text{C}$  following the method described by Simstich et al. [41] and Wu and Hillaire-Marcel [42]. A Finnigan MAT253 isotope ratio mass spectrometer with a Kiel III device was used for isotopic analysis at the University of Florida [43]. The

overall analytical reproducibility, as determined from replicate measurements on carbonate standards NBS-18, NBS-19, and an internal standard, is routinely better than  $\pm 0.08\%$  ( $\pm 1\sigma$ ) for  $\delta^{18}\text{O}$  [1]. Vital effects were corrected following the method of Stangeew [44] in which the equation,  $0.7\% \Delta\delta^{18}\text{O}$  (vital effect) =  $\delta^{18}\text{O}_{\text{Eq}} - \delta^{18}\text{O}_{\text{shell}}$ , was used for the modern oceanographic setting; however, accurate corrections must be different due to the imposition of the Arctic and Polar fronts during the glacial periods. In any case, the  $\delta^{18}\text{O}$  were used to construct the stratigraphy in which the marine isotope stages (MISs) were identified.

### 3.2.4. $^{14}\text{C}$ -AMS Dating

Five samples at different depths (Table 2) were selected in which each sample weigh  $>5000 \mu\text{g}$  of intact and clean *N. pachyderma* for  $^{14}\text{C}$  Accelerator Mass Spectrometry (AMS) dating. Samples were sent to the W. M. Keck Carbon Cycle AMS Facilities at the University of California in Irvine, USA. The  $^{14}\text{C}$ -AMS dates were calibrated to the calendar year before the present (1950) using the latest version of the radiocarbon calibration program CALIB 8.10 [45] in which the Marine20 reservoir ages were used [46].

**Table 2.**  $^{14}\text{C}$ -AMS dates and tie points used to construct the age model of core Hu90-08.

No.	Depth (cm)	Uncorrected $^{14}\text{C}$ Age (yr.) $\pm 1\sigma$ Error	Cal. ka BP $1\sigma$ Age Range	Species Used	Laboratory ID
1	10–12	$6532 \pm 20$	6.807	<i>G. bulloides</i>	
2	109–110	$17,960 \pm 40$	20.757	<i>N. pachyderma</i>	UCI-190945
3	161–162	$21,285 \pm 50$	24.591	<i>N. pachyderma</i>	UCI-190946
4	220–221	$31,270 \pm 140$	34.868	<i>N. pachyderma</i>	UCI-190947
5	310–311	$40,510 \pm 530$	42.851	<i>G. inflata</i>	UCI-219476
1 <sup>a</sup>	213		29.5 <sup>1</sup>		
2 <sup>a</sup>	440		59.5 <sup>1</sup>		
3 <sup>a</sup>	505		64 <sup>1</sup>		
4 <sup>a</sup>	595		70 <sup>1</sup>		
5 <sup>a</sup>	630		85.5 <sup>1</sup>		
6 <sup>a</sup>	655		88.5 <sup>1</sup>		
7 <sup>a</sup>	670		98 <sup>1</sup>		
8 <sup>a</sup>	730		110.5 <sup>1</sup>		
9 <sup>a</sup>	770		128 <sup>1</sup>		
10 <sup>a</sup>	780		130 <sup>1</sup>		
11 <sup>a</sup>	800		135 <sup>1</sup>		
12 <sup>a</sup>	815		139.5 <sup>1</sup>		
13 <sup>a</sup>	845		145.5 <sup>1</sup>		
14 <sup>a</sup>	885		149.5 <sup>1</sup>		

<sup>a</sup> Tie point; <sup>1</sup> Lisiecki and Stern [47].

### 3.2.5. Age Model Construction

The age model of the core Hu90-08 was constructed by employing two methods: (1) Using five  $^{14}\text{C}$ -AMS dates between 10.5 and 311 cm, and (2) constructing the oxygen isotope stratigraphy using the  $\delta^{18}\text{O}$  in *N. pachyderma* (Figure 3a) in which MISs were clearly identified. Fourteen tie points older than 40 ka (Figure 3) were obtained through matching with the deep North Atlantic benthic  $\delta^{18}\text{O}$  stack of Lisiecki and Stern [47]. A total of 19 control points were used to construct the age model in which linear sedimentation rates between the  $^{14}\text{C}$ -AMS dates/tie points are considered. As a result, it appears that the core Hu90-08 contains climate records between 3.54 and 145 ka for the depth interval between 0 and 841.5 cm (Figure 4). The estimated sedimentation rates vary between 1.62 and 8.5 cm/year, in which the Holocene period records the lowest sedimentation rates.

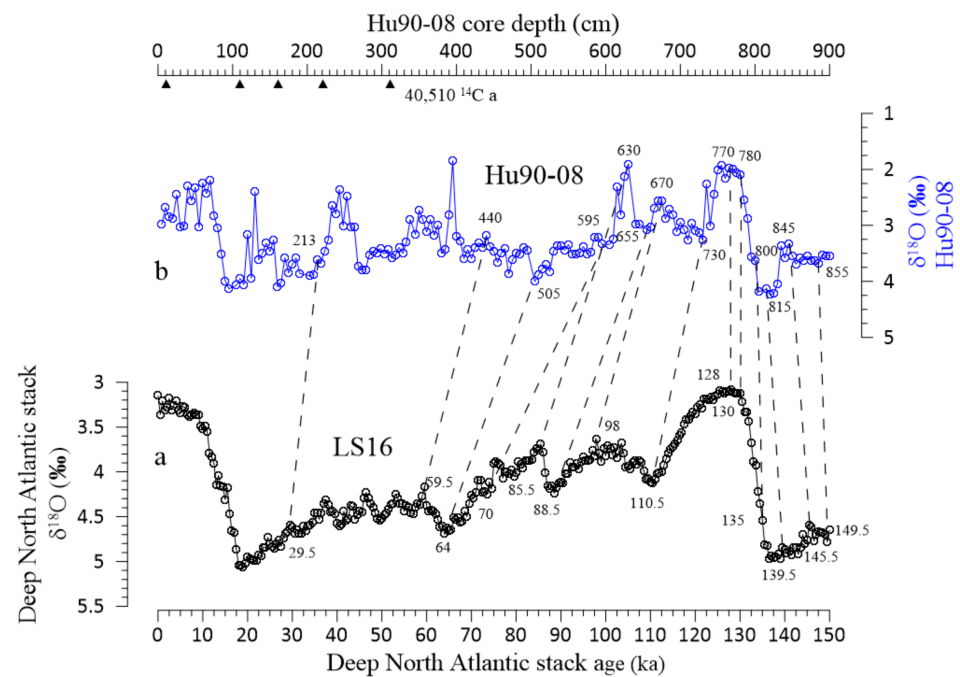


**Figure 3.** (a) Deep North Atlantic benthic foraminiferal  $\delta^{18}\text{O}$  stack [47] and (b)  $\delta^{18}\text{O}$  in the planktonic foraminifera *N. pachyderma* of core Hu90-08 (this study) are plotted. Fourteen tie points (Table 2) were obtained by visually aligning the  $\delta^{18}\text{O}$  values of Hu90-08 with those of the  $\delta^{18}\text{O}$  values of Lisiecki and Stern [47] and five  $^{14}\text{C}$ -Accelerator Mass Spectrometry (AMS) dates (Table 2) to construct the age model of core Hu90-08. Note that the upward triangles (b) denote the position of  $^{14}\text{C}$ -AMS dates.

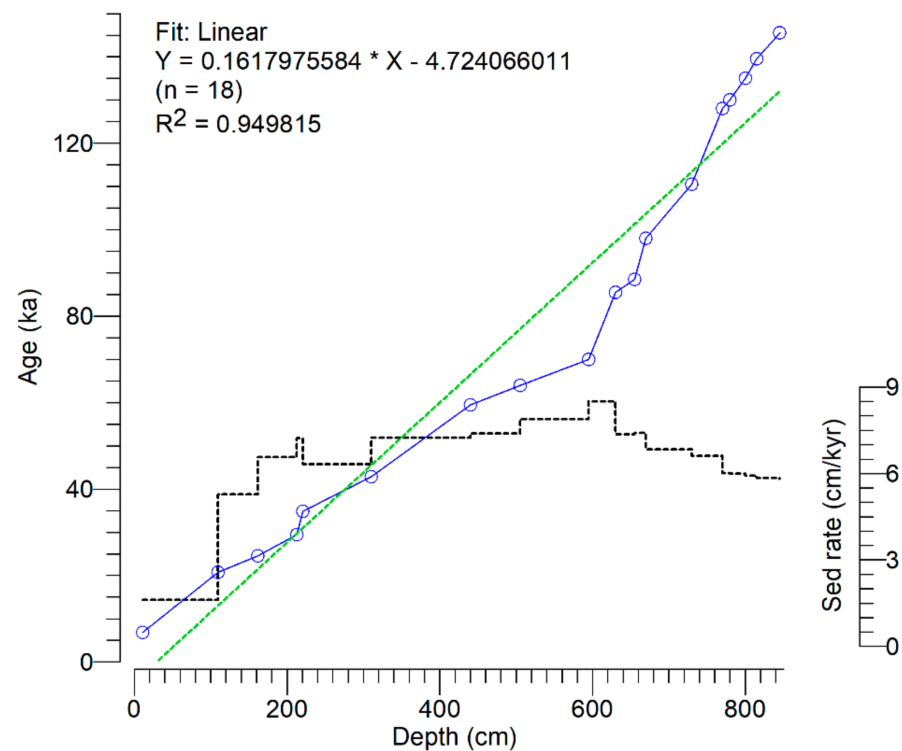


**Figure 4.** Age model of core Hu90-08 (this study) using the C14-AMS dates and tie points listed in Table 2. A linear fit (discontinuous green line) with the  $R^2 = 0.949815$  suggests a robust depth-age relationship, and the core contains climate records between 3.54 and 145 ka from 0 to 841.5 cm. Sedimentation rates range from 1.62 cm/kyr to 8.5 cm/kyr in which the Holocene period shows the lowest sedimentation rates.

### 4. Results

The IRD concentration varies between 24.75/g and 6483/g of dry sediments from 3.6 to 127.34 ka broadly divided into two periods (Figure 5b): The MIS5 (76–128 ka) in which the IRD is minimal (758/g); and the MIS2-4, high-frequency variable IRD with high IRD/g most of which are identified as the H-layers [1,48].

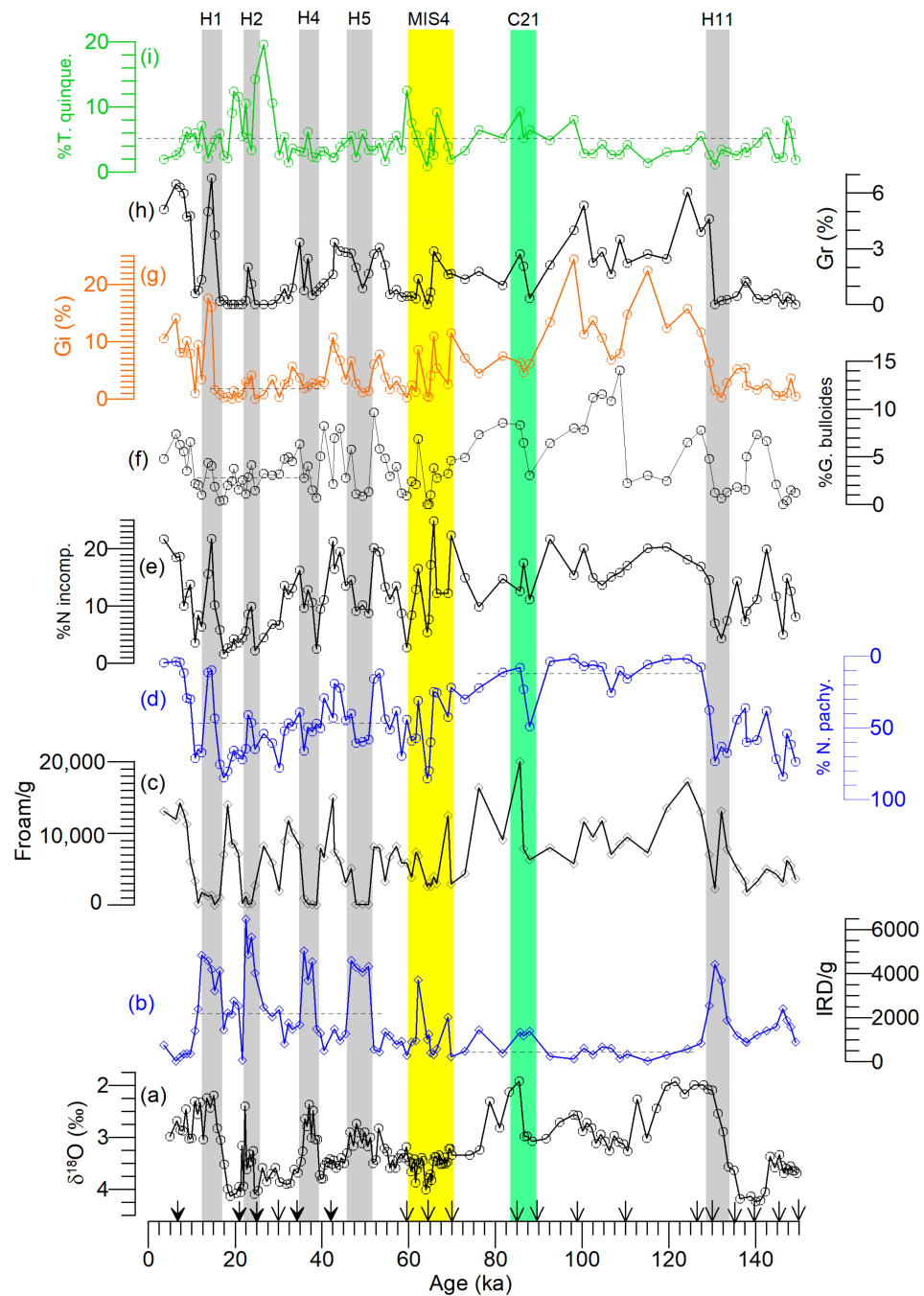


**Figure 5.** (a)  $\delta^{18}\text{O}$  in *N. pachyderma* and the concentration of (b) ice-rafted detritus (IRD/g) and (c) planktonic foraminifera (Foram/g) per gram of dry sediments in core Hu90-08 (this study). The percentage of six dominant foraminifera is plotted as shown from (d–i). Note the y-axis for %*N. pachyderma* is reversed (see detailed text). Downward filled-headed arrows represent the  $^{14}\text{C}$ -AMS dates used to construct the stratigraphy between 6.34 and 42.90 ka, whereas the simple-headed arrows show the tie points as illustrated in Figure 3. Note the yellow bar represents the MIS4. Hx = Heinrich events; Cx = Cooling events.

The total planktonic foraminiferal concentration varies from 6.1 to 20,018 shells/g (Figure 5c) between the cold MIS2-4 and warm MIS1 and 5 periods. The *Neogloboquadrina pachyderma*, *Neogloboquadrina incompta*, *Turborotalita quinqueloba*, *Globigerina bulloides*, and *Globorotalia inflata* are the important planktonic foraminifers comprising nearly 68.53% of the foraminifers' concentration (Figure 5). Both white and pink varieties of *Globigerinoides ruber* were also identified; however, due to the low concentration, i.e., 2.03%, it is not further discussed in detail in this study. The %*N. pachyderma* varies from 1.34 to 85.53% (Figure 5d) during the MIS2-4 with an increasing trend from 21.76 to 84.93%, whereas it is almost stable with <5% throughout the MIS5. The %*N. incompta* (Figure 5e) is high during the MIS5 and exhibits high-frequency variability in MIS3. Further, it appears that the low %*N. incompta* mostly matches with the high %*N. pachyderma*. The %*G. bulloides* (Figure 5f) and %*G. inflata* (Figure 5g) co-vary throughout the interval; however, their concentration remained relatively stable between 16 and 39 ka, although the concentration of the former is low compared to the latter and remained closed to the average of 5.45% (Figure 5g). The concentration of *T. quinqueloba* (Figure 5i) is mostly low, with an average of 4.71% except for the intervals 19.5 and 30 ka, in which it varies from 3.31 to 19.55%.

The  $\delta^{18}\text{O}$  in *N. pachyderma* ranges from 1.41 to 3.74‰ (Figure 5a) with an average of 3.0‰. The lightest  $\delta^{18}\text{O}$  were identified in the Holocene and MIS5a and 5e and the lighter peaks during the MIS2-3. The heaviest  $\delta^{18}\text{O}$  were found during MIS6 and MIS2, whereas the intermediate  $\delta^{18}\text{O}$  are found in MIS4.

H1, H2, H4, and H5 layers were identified by the IRD/g and %*N. pachyderma* peak and lighter  $\delta^{18}\text{O}$  in *N. pachyderma* in core Hu90-08 (Figure 5). The identification of H-layers is constrained by the  $^{14}\text{C}$ -AMS dates (Table 2). H11 was confidently identified at 128–134 ka by the high IRD/g and %*N. pachyderma* peak [4,25]. The minor IRD peak associated with the minor %*N. pachyderma* peak at 86–88 ka tentatively correlated to the cooling event C21 (Figure 5) of the North Atlantic [27,49].

## 5. Discussion

Changes in the subpolar gyre appear to have a tenuous link to the subtropical gyre of the North Atlantic during the past [50,51]. Depending on the thermal conditions of the mixed-layer and thermocline, this apparent link might have varied between weak and strong states. Data from core Hu90-08 illuminate on this link, which is broadly divided into four periods: Penultimate deglaciation including the termination II, MIS5, MIS3, and the last deglacial period including the Holocene. Five published records (Table 1), namely CH69-K09 [23], EW9303-37JPC (hereafter 37JPC; [24]), MD03-2664 [25,26], SU90-24 [19], and the Ocean Drilling Program (ODP) site 984 [27] in the subpolar gyre are plotted with Hu90-08 in Figures 6 and 7 as well, allowing us to provide an integrated assessment of broader changes in the sea-surface characteristics during the last glacial cycle. It should be stated a priori that some of the published records used in the study uses dated chronology due either to unavailability of the initial depth-scale data or  $^{14}\text{C}$ -dates/tie points or the unwillingness of the authors to share those data for unknown reasons. A two-pronged approach was employed to use those published data: publications in which depth-scale data are unavailable, for example, published  $\delta^{18}\text{O}$  from core 37JPC and benthic foraminifera  $\delta^{18}\text{O}$  for SU90-24, we used the dated age models. In contrast to cores 37JPC and SU90-24, data from cores CH69-K09, 984, and MD03-2664 are updated following our age-model construction protocol (see Section 3.2.5).

In terms of choosing proxies used to correlate among the records illustrated in Figures 6 and 7, two approaches were employed. The most commonly used proxies that reflect changes in the sea-surface, namely the IRD/g, %*N. pachyderma*, and %*T. quinqueloba* is used for the MIS5-4 period (Figure 6). Unavailability of *N. incompta*, *G. bulloides*, and *G. inflata* census data from cores 37JPC, MD03-2664, and 984 prevented us from making a similar correlation for MIS5-4 as was carried out for MIS3-2 (Figure 7). It should be stated that the IRD/g and %*N. pachyderma* are used as a common guide for both warm (MIS5 and

I) and cold (MIS4-2) in assessing cold and freshwater input into the subpolar gyre of the North Atlantic [27,52].

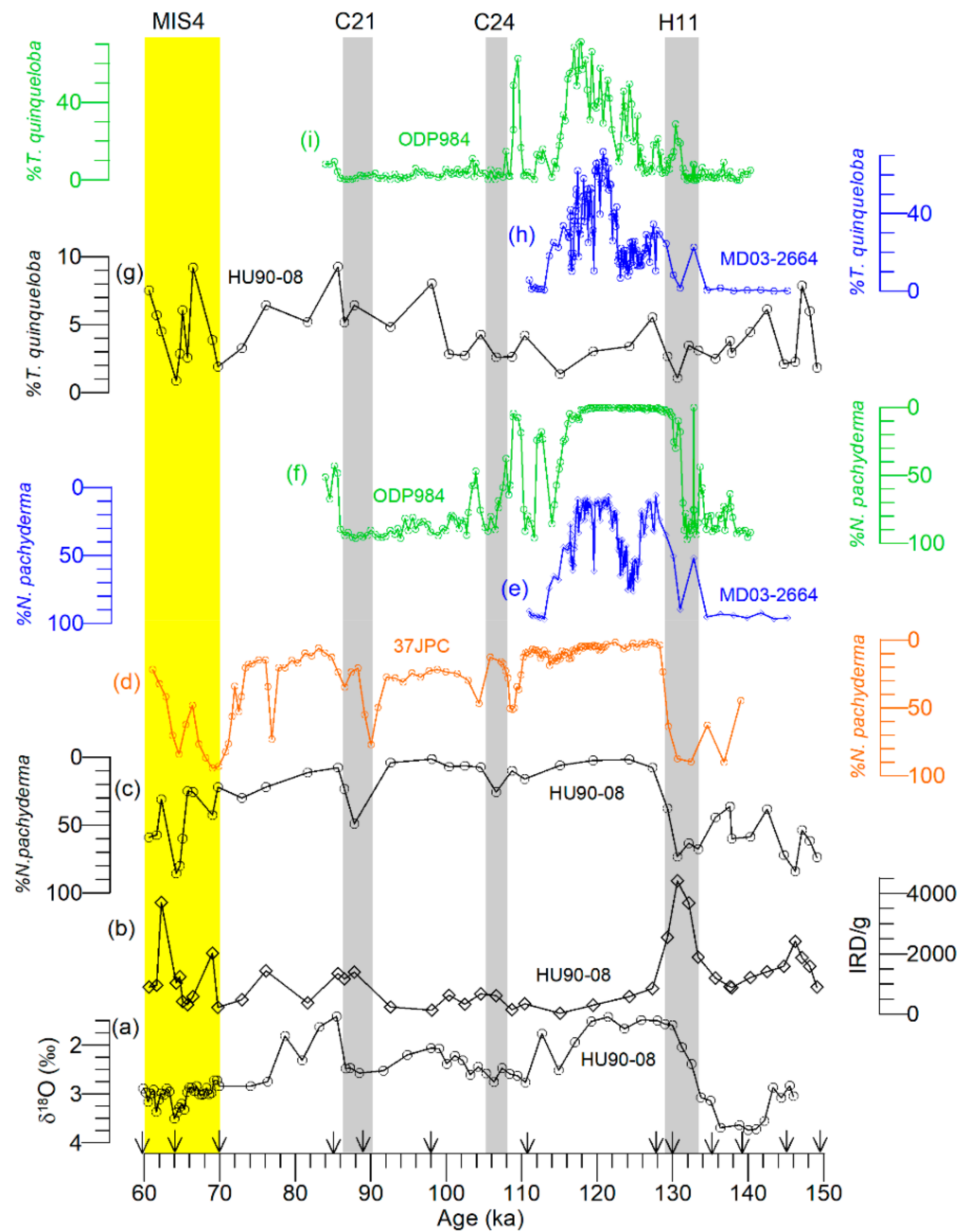


**Figure 6.** Paleo-proxy records of changes (a–i) in the sea-surface characteristics of the subpolar North Atlantic between 60 and 150 ka. Downward simple-headed triangles exhibit the tie points used to construct the age model of core Hu90-08 (this study). The vertical discontinuous line represents termination II (TII). Hx = Heinrich events; Cx = Cooling events.

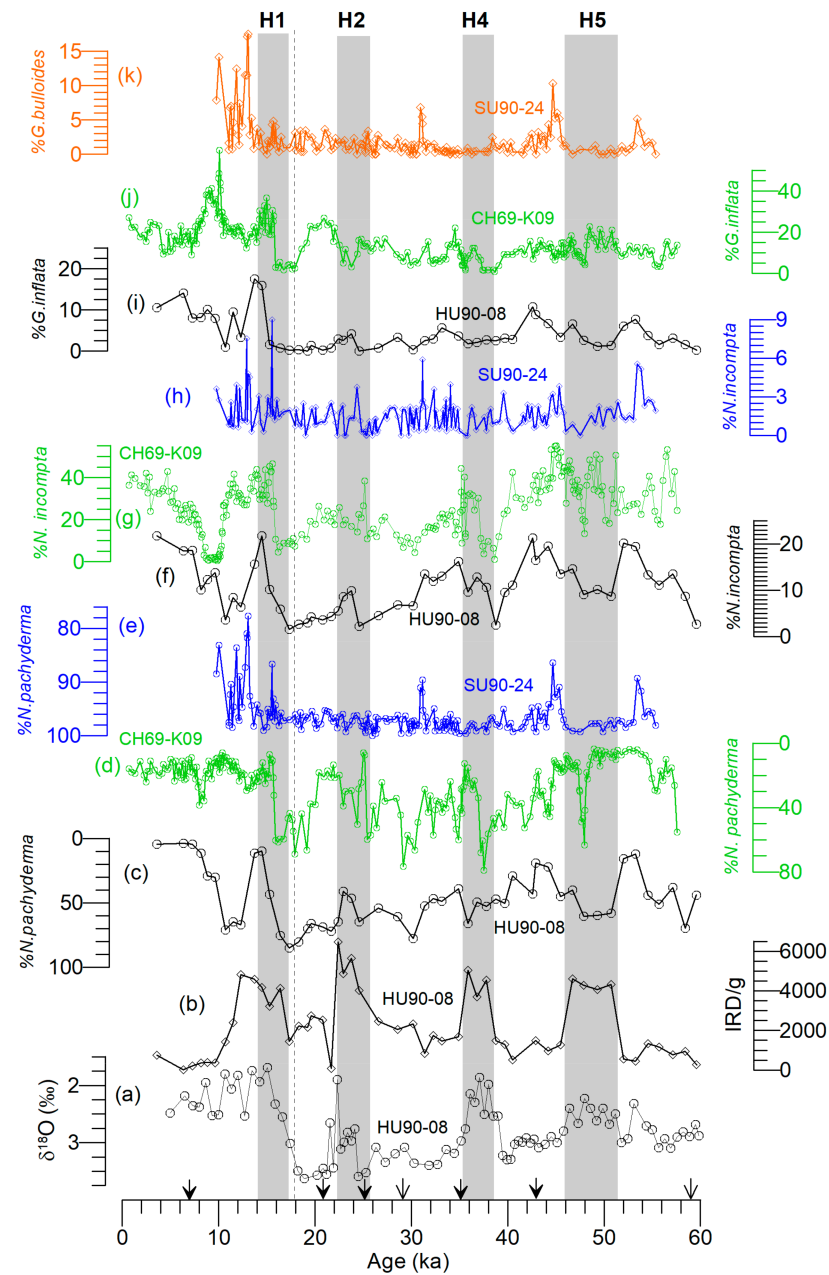


**Figure 7.** Proxy records of changes in the subpolar North Atlantic from cores Hu90-08 (black), CH69-K09 (green), and SU90-24 (blue) between 0 and 60 ka. (a,b) are the same as in Figure 5; however, %N. pachyderma (c–e), %N. incompta (f–h) and %G. inflata (i,j) of cores Hu90-08, CH69-K09, and SU90-24 are plotted. %G. bulloides (k) from core SU90-24 is independently plotted. Downward filled and unfilled headed triangles exhibit the  $^{14}\text{C}$ -AMS dates and tie points, respectively, used to construct the age model of core Hu90-08 (this study). Two published records, namely SU90-24 [19] and CH69-K09 [23], were also plotted to provide an integrated assessment of the western subpolar gyre. Note the vertical discontinuous line represents the termination I (TI), whereas the Hx = Heinrich events.

### 5.1. The penultimate Deglaciation (129.5 to 125 ka) in the Newfoundland Basin

The penultimate deglacial sequence, including the H11 in core Hu90-08, is similar to the sequence of events on core 37JPC [24]. The concentration of *N. pachyderma* is >80%, with traces of *T. quinqueloba*, *N. incompta*, *G. bulloides*, and *G. inflata* during H11 (Figures 5 and 6). The rapid heavy to light  $\delta^{18}\text{O}$  shift in core Hu90-08 (Figure 4) is consistent with the  $\delta^{18}\text{O}$  change in *N. pachyderma* of cores CH69-K09 [23] and MD03-2664 [52]. The shift in the  $\delta^{18}\text{O}$  reflects changes in the sea-surface freshening, suggesting the reorganization of the deep-

water masses through North Atlantic Deep-Water formation, as recorded by the benthic foraminiferal carbon isotopes from the nearby records [53,54]. A few lighter  $\delta^{18}\text{O}$  in *N. pachyderma* within the penultimate deglaciation on the southern Greenland margin [35,55] were attributed to the Greenland Ice Sheet (GIS) meltwater discharge. However, the lighter  $\delta^{18}\text{O}$  events appear to be absent on the high-resolution Eirik Drift records [25,52], which might be either due to the limited spatial influence of the meltwater or a mismatch between the age models. In any case, if these events were not recorded on the high-resolution Eirik Drift sites (Figure 1), it is implausible that those events will be recorded either in core 37JPC or Hu90-08 (this study) due to the coarse temporal resolution or dissipation of the meltwater signatures at those sites. However, Winsor et al. [55] and Carlson et al. [35] provided an alternative explanation suggesting that the sustained cold and fresh East Greenland Current may have suppressed the  $\delta^{18}\text{O}$  from ~128 ka onward at site MD99-2227 (Figure 1), which cannot be tested at site Hu90-08 at present due to coarse temporal resolution.

The high IRD/g and %*N. pachyderma* peak with the concomitant decrease in %*N. incompta* in H11 of core Hu90-08 (Figure 6) suggest that the ice-rafting and meltwater were discharged. The precipitous decrease from 14.54% to near absent *N. incompta* and traces of *G. inflata* and *T. quinqueloba* suggests the impact of prevailing meltwater and the absence of seasonal subpolar water. In core 37JPC [~300 km from the SE Grand Banks coast], the 95% *N. pachyderma* and 683 lithics/g with the trace *T. quinqueloba* in H11 suggest that widespread ice-rafting during H11 in the Newfoundland Basin [24]. Carlson et al. [35] reported a  $\text{CaCO}_3$  (%) peak and Fe and Ti trough using the XRF-scanner data for H11, where the authors attributed it to the GIS discharge. An IRD/g and %*N. pachyderma* peak with the lighter  $\delta^{18}\text{O}$  in *N. pachyderma* and *Cibicides wuellerstorfi* was also reported for H11 in core MD03-2664 [25,52,54]. The authors suggested that such changes in the planktonic and benthic foraminifers reflect the meltwater impact. However, such  $\delta^{18}\text{O}$  shift was not found in cores 37JPC or Hu90-08, most likely due to the coarse temporal resolution of the latter records or spatial difference in response to the meltwater.

### 5.2. Sea-Surface Characteristics during the MIS5

The lightest  $\delta^{18}\text{O}$  in *N. pachyderma* of 1.41‰ at 125.81 ka is considered the onset of MIS5e in which both *N. incompta* and *G. bulloides* present the highest values and the concentration of *N. pachyderma* is <5% (Figure 6). Throughout the MIS5, two prominent cold events labeled as C24 and C21 [49], in which a minor IRD peak was tied to the latter cold event. Mokeddam et al. [27] identified six cooling events between H11 and C24, including three minor events within C27 (a, b and c) on the eastern subpolar gyre. The authors used the *N. pachyderma*, *T. quinqueloba*, and *N. incompta* to assess migration of the Polar and Arctic fronts from 102 to 134 ka. The %*N. pachyderma* at sites Hu90-08 and 984 during MIS5e-c is identical; however, the extent and magnitude of concentration of *T. quinqueloba* and *N. incompta* vary between 0 and 71% and 0.38 and 45.31%, respectively, at site 984, reflecting a strong influence by the subpolar water mass. In contrast to site 984, the %*T. quinqueloba* and %*N. incompta* at site Hu90-08 vary between 0.86 and 9.28% and 4.33 and 24.92%, respectively, suggesting a strong influence by the warm and salty NAC. Irvali et al. [52] also reported the %*T. quinqueloba* and %*N. incompta* from 110 and 135 ka at MD03-2664 (Figure 6), in which the millennial-scale variability recorded in the eastern subpolar gyre (at site 984) appears to be subtle or absent. Further, an IRD peak centered at 117 ka in the western subpolar gyre (at MD03-2664) is also absent at sites Hu90-08 and 984, suggesting the regional nature of the 117-ka event. In short, there are heterogeneities between the eastern and western subpolar gyre and intra-western subpolar gyre (i.e., between the SE Grand Banks and eastern Newfoundland Basin) during the MIS5e-c. These differences most likely reflect the extent to which the Labrador Current and NAC injected cold and freshwater versus warm and salty water, respectively, to the subpolar gyre.

A millennial-scale cooling event at 125 ka (between ~126 and 124 ka) within the warmest MIS5e was identified by the %*N. pachyderma* from 18 to 76%, decrease in %*N. incompta*, and %*G. bulloides* on the Eirik Drift [25,52]) suggesting the influence by the polar

water compared to the subpolar water. The SST was cooled by 3.4 °C in the Mg/Ca-temperature in *N. pachyderma* during this event, which could be attributed to ice-rafting-derived meltwater; however, there was no abrupt increase in the IRD associated with this event. Irvani et al. [25,52] also reported a ~0.8% decrease in  $\delta^{18}\text{O}$  in *N. pachyderma*, which implied to the authors the existence of fresher near-surface conditions. Galaasen et al. [53] reported lighter benthic foraminiferal  $\delta^{13}\text{C}$  during this event and suggested a slowing down of the North Atlantic Deep-Water formation. This cooling event appears to be absent in core Hu90-08, which might be due to the coarse data resolution, or the cooling event was minimized by the interference of the warm NAC inflow, consistent with the absence of cooling signature in core 37JPC (Figure 6). A minor dip in the  $\delta^{18}\text{O}$  in core Hu90-08 could be correlative to that cooling event; however, we refrained from interpreting this single datum any further.

### 5.3. Sea-Surface Characteristics during the MIS4-MIS3

The C24 cooling event centered at 106.5 ka in core Hu90-08 corresponds to the sharp rise in the %*N. pachyderma* in the eastern subpolar gyre (Figure 6). A similar peak in %*N. pachyderma* at 109.5 ka also found in core 37JPC, although there appears to be an offset in age between the two records (i.e., 37JPC and Hu90-08), most likely due to the use of outdated age model [56] in core 37JPC. An intermediate IRD peak at 88 ka with a concomitant rise in the %*N. pachyderma* (Figure 6) is correlated to the cooling event C21 for the first time in the western subpolar gyre. The lighter  $\delta^{18}\text{O}$  event appears to follow the IRD event suggesting freshening of the sea-surface.

The IRD/g and %*N. pachyderma* peaks identify H2, H4, and H5 [57] with the concomitant light  $\delta^{18}\text{O}$ , although there are differences in  $\delta^{18}\text{O}$  during each H-event (Figure 7). One of the striking features is the covariation of the foraminifers/g with that of the abrupt rise in IRD/g, consistent with the hypothesis of a near-collapse of the productivity [5,58]. The highest concentration (85%) of *N. pachyderma* but significant reduction in *N. incompta*, *T. quinqueloba*, *G. bulloides*, and *G. inflata* during H-events (Figure 5) suggests an incursion by the polar water. Moreover, the decline of *N. pachyderma* but an increase in *N. incompta* immediately after the H-events reflects rapid changeover by the subpolar to transitional water at site Hu90-08. The lighter *N. pachyderma*  $\delta^{18}\text{O}$  suggests a sea-surface freshening during the H2, H4, and H5, consistent with the records at other regional sites (Figures 1 and 7). de Vernal et al. [38] reported SSTs, sea-surface salinities, and sea-ice covers during the H0, H1, and H2, including the LGM (Figure 1; Table 1). The authors reported 0 °C and <5 °C SSTs during February and August, respectively, with sea-ice cover ranging from 4 to 12 months/year. Our data are consistent with the broader temperature aspect of de Vernal et al. [38] when the transfer function of %*N. pachyderma* to SST [59] is applied. Elliot et al. [19] also reported the concentration of *N. pachyderma* (Figure 7e), which remained ~95% during the MIS3 in the Irminger Basin, suggesting an absolute dominance by the polar water mass. By developing a Heinrich variable (RM), Hiscott et al. [10] reported the intensity of ice-rafting on the sea-surface, matching with the summer and winter SSTs. However, the exact mechanism by which the ice-rafting (i.e., meltwater discharge) and the rise in the SSTs were linked remains unclear.

The IRD records at Hu90-08 (Figure 7) are consistent with the H1, H2, H4, and H5 ice-rafting records from the nearby core SU90-11 [60], except for two minor IRD peaks within the MIS4 in Hu90-08. An increasing trend from 20 to 85.5% in *N. pachyderma* between 54 and 10 ka (Figure 7), a mirror image to the %*N. incompta* might reflect a gradual sea-surface cooling and more frequent incursions by the polar water during the winter and spring times [10,59]. This longer-scale inverse covariation between the %*N. pachyderma* and %*N. incompta* was frequently interrupted by the H-events. In contrast to the incursion by the polar water, the increase in %*N. incompta* (Figure 5) suggests frequent incursions by the warm and salty water due to the NAC inflow, most likely during the late spring and summer. The high-frequency variability in %*T. quinqueloba* ranging from 0.86 to 19.55%

suggests occasional intrusions by the subpolar water [27] at site Hu90-08, most likely due to the penetration of the glacial Labrador Current [1,61].

In contrast to the records at site Hu90-08, the %*N. pachyderma* peaks in the millennial-scale records of CH69-K09 due to its higher temporal resolution are narrower, implying that the impact of H-events-induced meltwater lasted for a short period. Granted that there might be a mismatch between the age models of cores, however, a close inspection reveals much more subtle changes. For example, the core top sample of CH69-K09 contains 15.80% polar species (*N. pachyderma*), 71.46% transitional subarctic species (*N. incompta*, *G. bulloides*, and *G. inflata*), and ~10% tropical and subtropical species (*Orbulina universa*, *G. ruber pink* and *white*, and *G. sacculifer*). The presence of these species most likely reflects occasional influence by the warm NAC inflow. In contrast to core CH69-K09, subtropical and subtropical species constitute 4.47%, 37.06% transitional species, and <7% *N. pachyderma* in the core top of site Hu90-08. Further, the overall %*N. pachyderma* is higher in Hu90-08 than that of CH69-K09 during the MIS3 (Figure 7). Lighter  $\delta^{18}\text{O}$  during H4, H2, and H1 in *G. bulloides* and *N. pachyderma*, respectively, reflect the impact of meltwater on the mixed-layer and thermocline at site CH69-K09. Such evaluation in  $\delta^{18}\text{O}$  between the *G. bulloides* and *N. pachyderma* during H-events cannot be assessed due to the unavailability of data in Hu90-08. On the basis of the IRD and *N. pachyderma* peaks and  $\delta^{18}\text{O}$ , it could be summarized that the sudden invasion by the meltwater freshened the sea-surface during the H-events in the western subpolar gyre (Newfoundland Basin).

#### 5.4. The Last Deglacial Climate (including the Holocene) in the Western Subpolar Gyre

The onset of the last deglacial period is marked by the heavy to lighter  $\delta^{18}\text{O}$  shift at 19 ka at site Hu90-08 (Figure 7). The prominent IRD/g and %*N. pachyderma* peak without the distinct lighter  $\delta^{18}\text{O}$ , as observed for other H-events in Hu90-08, is most likely due to the competing factors between the rise of the Northern Hemisphere insolation [62] and invasion by the warm and salty water due to the NAC inflow. The abrupt rise of %*N. incompta* and %*G. inflata* with the rapid fall in %*N. pachyderma* at 16.5 ka provides support for this hypothesis of climate amelioration in the western subpolar gyre. Such an invasion by the warm and salty waters must have been restricted to the western subpolar gyre, as revealed by the absence of a rise in %*N. incompta*, *G. inflata*, or *G. bulloides* in the Irminger Basin (at site SU90-24; Figure 7). The %*N. pachyderma* and the absence of an IRD peak centered at 12 ka (Figure 7) might correlate to the Younger Dryas (YD) cooling event, consistent with the other open North Atlantic paleo-proxy records of the YD [38,63,64]. It appears that changes related to the YD event were not recorded either in the Irminger Basin (at SU90-24) or at the foot of the Newfoundland slope (at CH69-K09), consistent with the dynamics of the Coriolis force in the Northern Hemisphere and freshwater movement [65,66].

The Holocene record in Hu90-08 is short, amounting to ~50 cm compared to the MIS3 or MIS5, consistent with the thickness of Holocene sediments to the broader deep Labrador Sea [34,48]. The IRD/g is very poor, similar to the concentration of IRD/g during the MIS5e-c, reflecting either very little icebergs appearance at the core site or less iceberg discharge from the GIS or less transport of Arctic sea-ice. The %*N. pachyderma* declines from 71.12 to 4.47%, whereas an increase in %*T. quinqueloba* compared to the MIS3/2 reflects changes in the Polar to Arctic Front (Figure 5). This finding is similar to the eastern subpolar gyre (at site 984). A similar rising trend from 10.71 to 3.60 ka in %*G. bulloides* and *G. inflata* suggests changes from Polar to Arctic Front, consistent with the trends in %*N. pachyderma* and %*T. quinqueloba* (Figure 5i).

Bond et al. [67] used sediment cores west of core Hu90-08 to document changes in the surface water properties during the Holocene. Hoogakker et al. [68] applied the Mg/Ca-SST to the *G. bulloides* to report sub(surface) water conditions to assess the impact of freshwater on the Labrador Sea Water formation during the early Holocene (at MD95-2024). The absence of abundance data of *G. bulloides* data at site MD95-2024 raises the question about the extent to which sea-surface condition was recorded. For example, Stangeew [37] reported that *N. pachyderma* was the most abundant in the upper 0–50 m,

whereas *T. quinqueloba* showed a variable distribution with a maximum in 0–200 m with traces of *G. bulloides* from the multinet plankton tows, very close to core MD95-2024. In addition, the %*G. bulloides* in Hu90-08 vary between 2.19 and 6.30% during the Holocene (Figure 5), suggesting limited applicability to the use of *G. bulloides* in paleoceanographic reconstruction in the western subpolar gyre.

## 6. Conclusions

Changes in the sea-surface characteristics, namely the ice-rafting, meltwater discharge, and sea-surface temperatures, were reconstructed for the last 145,000 years using a sediment core Hu90-08 retrieved from the Milne seamount of the northwest Atlantic Ocean. Foraminiferal assemblage data in conjunction with the oxygen isotopes in *Neogloboquadrina pachyderma* suggest rapid turnover of the upper water masses, switching between the polar and subpolar waters. These changes were rapid during the abrupt climate events of the MIS3, whereas such changes are either subtle or absent during the MIS5.

Five Heinrich H1, H2, H4, H5, and H11 layers were identified by the high IRD/g and %*N. pachyderma* peak and traces of the subpolar species *N. incompta*, *G. bulloides*, and *G. inflata* suggest complete dominance by the polar water masses. The decline of *N. pachyderma* but the rise of *N. incompta* immediately after the H-events suggests a return of the subpolar water masses.

The anti-covariation of %*N. pachyderma* with the %*N. incompta* provides an indirect proxy for the sea-surface temperatures in which the former dominates in less than 8 °C, whereas the latter thrive at an optimal temperature of 12 °C. Such rapid changes in the western subpolar gyre reflect a close interaction between the cold and fresh Labrador Current and warm and salty North Atlantic Current.

**Author Contributions:** Conceptualization, H.R.; methodology, H.R., Q.Q.L., and M.Z.; software, Z.W.Z.; validation, Y.W., Z.W.Z., and H.R.; formal analysis, Y.W.; investigation, M.Z., and Q.Q.L.; resources, H.R.; data curation, H.R. and Y.W.; writing—original draft preparation, H.R.; writing—review and editing, Q.Q.L., Y.W., and M.Z.; visualization, Z.W.Z.; supervision, H.R.; project administration, M.Z. and H.R.; funding acquisition, H.R. All authors have read and agreed to the published version of the manuscript.

**Funding:** This research was funded by the natural science foundation of China, grant number 41776064, and the Atlantic Canada opportunities agency, grant number 204567. The Shanghai Ocean University funded the APC.

**Data Availability Statement:** Data used in this article can be found at [http://ed.gdr.nrcan.gc.ca/index\\_e.php](http://ed.gdr.nrcan.gc.ca/index_e.php).

**Acknowledgments:** Part of the study conducted when the senior author was at The Ohio State University and Memorial University of Newfoundland. Samples used in this study were collected by the joint Memorial University of Newfoundland and Geological Survey of Canada (Atlantic) cruise #Hu9007. We wish to acknowledge the captain, crews, and laboratory personnel for their support. HR also acknowledges help from David J.W. Piper and Kate Jarrett at the Geological Survey of Canada (Atlantic).

**Conflicts of Interest:** The authors declare no conflict of interest. The funders had no role in the design of the study, in the collection, analyses, or interpretation of data, in the writing of the manuscript, or in the decision to publish the results.

## References

1. Rashid, H.; Piper, D.J.W.; MacKillop, K.; Ouellette, D.; Vermooten, M.; Muñoz, A.; Jiménez, P. Dynamics of sediments on a glacially influenced, sediment starved, current-swept continental margin: The SE Grand Banks Slope off Newfoundland. *Mar. Geol.* **2019**, *408*, 67–86. [CrossRef]
2. Andrews, J.T.; Tedesco, K. Detrital carbonate-rich sediments, northwestern Labrador Sea: Implications for ice-sheet dynamics and iceberg rafting (Heinrich) events in the North Atlantic. *Geology* **1992**, *20*, 1087–1090. [CrossRef]
3. Rashid, H.; Hesse, R.; Piper, D.J.W. Origin of unusually thick Heinrich layers in ice-proximal regions of the northwest Labrador Sea. *Earth Planet. Sci. Lett.* **2003**, *208*, 319–336. [CrossRef]

4. Heinrich, H. Origin and consequences of cyclic ice rafting in the northeast Atlantic Ocean during the past 130,000 years. *Quat. Res.* **1988**, *29*, 143–152. [[CrossRef](#)]
5. Bond, G.C.; Heinrich, H.; Broecker, W.S.; Labeyrie, L.; McManus, J.; Andrews, J.; Huon, S.; Jantschik, R.; Clasen, S.; Simet, C.; et al. Evidence for massive discharges of icebergs into the North Atlantic Ocean during the last glacial period. *Nature* **1992**, *360*, 245–261. [[CrossRef](#)]
6. Dansgaard, W.; Johnsen, S.J.; Clausen, H.B.; Dahl-Jehnsen, D.; Gundestrup, N.S.; Hammer, C.U.; Hvidberg, C.S.; Stejensen, J.P.; Sveinbjörnsdóttir, A.E.; Jouzel, J.; et al. Evidence for general instability of past climate from a 250-kyr ice-core record. *Nature* **1993**, *364*, 218–220. [[CrossRef](#)]
7. Boyle, E.A. Is ocean thermohaline circulation linked to abrupt stadial/interstadial transitions? *Quat. Sci. Rev.* **2000**, *19*, 255–272. [[CrossRef](#)]
8. Lohmann, G.; Butzin, M.; Eissner, N.; Shi, X.-X.; Stepanek, C. Abrupt Climate and Weather Changes Across Time Scales. *Paleoceanogr. Paleoclimatol.* **2020**, *35*, e2019PA003782. [[CrossRef](#)]
9. Stoner, J.S.; Channell, J.E.T.; Hillaire-Marcel, C.; Kissel, C. Geomagnetic paleointensity and environmental record from Labrador Sea core MD95-2024: Global marine sediment and ice core chronostratigraphy for the last 110 kyr. *Earth Planet. Sci. Lett.* **2000**, *183*, 161–177. [[CrossRef](#)]
10. Hiscott, R.N.; Aksu, A.E.; Mudie, P.J.; Parsons, D.F. 2001. A 340,000 years record of ice rafting, palaeoclimatic fluctuations, and shelf-crossing glacial advances in the southwestern Labrador Sea. *Glob. Planet. Chang.* **2001**, *28*, 227–240. [[CrossRef](#)]
11. Channell, J.E.T.; Hodell, D.A.; Romero, O.; Hillaire-Marcel, C.; de Vernal, A.; Stoner, J.S.; Mazaud, A.; Röhl, U. A 750-kyr detrital-layer stratigraphy for the North Atlantic (IODP Sites U1302–U1303, Orphan Knoll, Labrador Sea). *Earth Planet. Sci. Lett.* **2012**, *317–318*, 218–230. [[CrossRef](#)]
12. Hodell, D.A.; Channell, J.E.T.; Curtis, J.H.; Romero, O.E.; Röhl, U. Onset of “Hudson Strait” Heinrich events in the eastern North Atlantic at the end of the middle Pleistocene transition (~640 ka)? *Paleoceanography* **2008**, *23*. [[CrossRef](#)]
13. Hodell, D.A.; Nicholl, J.A.; Bontognali, T.R.R.; Danino, S.; Dorador, J.; Dowdeswell, J.A.; Einsle, J.; Kuhlmann, H.; Martrat, B.; Mleneck-Vautravers, M.J.; et al. Anatomy of Heinrich Layer 1 and its role in the last deglaciation. *Paleoceanography* **2017**, *32*, 284–303. [[CrossRef](#)]
14. Stein, R.; Hefter, J.; Grützner, J.; Voelker, A.; Naafs, B.D.A. Variability of surface water characteristics and Heinrich-like events in the Pleistocene midlatitude North Atlantic Ocean: Biomarker and XRD records from IODP Site U1313 (MIS 16–9). *Paleoceanography* **2009**, *24*, PA2203. [[CrossRef](#)]
15. Naafs, B.D.A.; Hefter, J.; Acton, G.; Haug, G.H.; Martínez-García, A.; Pancost, R.; Stein, R. Strengthening of North American dust sources during the late Pliocene (2.7 Ma). *Earth Planet. Sci. Lett.* **2012**, *317–318*, 8–19. [[CrossRef](#)]
16. Bond, G.C.; Broecker, W.S.; Johnsen, S.J.; McManus, J.; Labeyrie, L.; Jouzel, J.; Bonani, G. Correlations between climate records from North Atlantic sediments and Greenland Ice. *Nature* **1993**, *365*, 143–147. [[CrossRef](#)]
17. Ruddiman, W.F. Late Quaternary deposition of ice-rafted sand in the sub-polar North Atlantic (40°–65° N). *Geol. Soc. Am. Bull.* **1977**, *88*, 1813–1821. [[CrossRef](#)]
18. Oppo, D.W.; Lehman, S.J. Suborbital timescale variability of north Atlantic deep water during the past 200,000 years. *Paleoceanography* **1995**, *10*, 901–910. [[CrossRef](#)]
19. Elliot, M.; Labeyrie, L.; Bond, G.; Cortijo, E.; Turon, J.-L.; Tisnerat, N.; Duplessy, J.-C. Millennial-scale iceberg discharges in the Irminger basin during the last glacial period: Relationship with the Heinrich events and environmental settings. *Paleoceanography* **1998**, *13*, 433–446. [[CrossRef](#)]
20. Hodell, D.A.; Evans, H.F.; Channell, J.E.T.; Curtis, J.H. Phase relationships of North Atlantic ice-rafted debris and surface-deep climate proxies during the last glacial period. *Quat. Sci. Rev.* **2010**, *29*, 3875–3886. [[CrossRef](#)]
21. Dokken, T.M.; Nisancioglu, K.H.; Li, C.; Battisti, D.S.; Kissel, C. Dansgaard-Oeschger cycles: Interactions between ocean and sea ice intrinsic to the Nordic seas. *Paleoceanography* **2013**, *28*, 491–502. [[CrossRef](#)]
22. Barker, S.; Chen, J.; Gong, X.; Jonkers, L.; Knorr, G.; Thornalley, D. Icebergs not the trigger for North Atlantic cold events. *Nature* **2015**, *520*, 333–336. [[CrossRef](#)]
23. Labeyrie, L.; Leclaire, H.; Waelbroeck, C.; Cortijo, E.; Duplessy, J.-C.; Vidal, L.; Elliot, M.; Coat, B.L.; Auffret, G. Temporal Variability of the Surface and Deep Waters of the North West Atlantic Ocean at Orbital and Millennial Scales. *Mech. Glob. Clim. Chang. Millenn. Time Scales* **1999**, *112*, 77–98.
24. McManus, J.F.; Oppo, D.W.; Keigwin, L.D. Thermohaline Circulation and Prolonged Interglacial Warmth in the North Atlantic. *Quat. Res.* **2002**, *58*, 17–21. [[CrossRef](#)]
25. Irvani, N.; Ninnemann, U.S.; Galaasen, E.V.; Rosenthal, Y.; Kroon, D.; Oppo, D.W.; Kleiven, H.F.; Darling, K.F.; Kissel, C. Rapid switches in subpolar North Atlantic hydrography and climate during the Last Interglacial (MIS 5e). *Paleoceanography* **2012**, *27*. [[CrossRef](#)]
26. Irvani, N.; Ninnemann, U.S.; Kleiven, H.F.; Galaasen, E.V.; Morley, A.; Rosenthal, Y. Evidence for regional cooling, frontal advances, and East Greenland Ice Sheet changes during the demise of the last interglacial. *Quat. Sci. Rev.* **2016**, *150*, 184–199. [[CrossRef](#)]
27. Mokeddem, Z.; McManus, J.F.; Oppo, D.W. Oceanographic, dynamics and the end of the last interglacial in the subpolar North Atlantic. *Proc. Natl. Acad. Sci. USA* **2014**, *111*, 11263–11268. [[CrossRef](#)]
28. Cuny, J.; Rhines, P.B.; Niiler, P.P.; Bacon, S. Labrador Sea boundary currents and the fate of the Irminger Sea Water. *J. Phys. Oceanogr.* **2002**, *32*, 627–647. [[CrossRef](#)]

29. Zantopp, R.; Fischer, J.; Visbeck, M.; Karstensen, J. From interannual to decadal: 17 years of boundary current transports at the exit of the Labrador Sea. *J. Geophys. Res. Ocean.* **2017**, *122*, 1724–1748. [CrossRef]
30. Rossby, T. The North Atlantic current and surrounding waters: At the crossroads. *Rev. Geophys.* **1996**, *34*, 463–481. [CrossRef]
31. Mertens, C.; Rhein, M.; Walter, M.; Böning, C.W.; Behrens, E.; Kieke, D.; Steinfeldt, R.; Stöber, U. Circulation and transports in the Newfoundland Basin, western subpolar North Atlantic. *J. Geophys. Res. Ocean.* **2014**, *119*, 7772–7793. [CrossRef]
32. Schlitzer, R. Data analysis and visualization with ocean data view. *CMOS Bull. SCMO* **2015**, *43*, 9–13.
33. Zhuravleva, A.; Bauch, H.A.; Nieuwenhove, N.V. Last Interglacial (MIS 5e) hydrographic shifts linked to meltwater discharges from the East Greenland margin. *Quat. Sci. Rev.* **2017**, *164*, 95–109. [CrossRef]
34. Hillaire-Marcel, C.; de Vernal, A.; Bilodeau, G.; Wu, G. Isotope stratigraphy, sedimentation rates, deep circulation, and carbonate events in the Labrador Sea during the last ~200 kyr. *Can. J. Earth Sci.* **1994**, *31*, 63–89. [CrossRef]
35. Carlson, A.E.; Clark, P.U. Rapid climate change and Arctic Ocean freshening: Comment. *Geology* **2008**, *36*, e177. [CrossRef]
36. Oppo, D.W.; McManus, J.F.; Cullen, J.L. Evolution and demise of the Last Interglacial warmth in the subpolar North Atlantic. *Quat. Sci. Rev.* **2006**, *25*, 3268–3277. [CrossRef]
37. Chapman, M.R.; Shackleton, N.J. Global ice-volume fluctuations, North Atlantic ice-rafting events, and deep-ocean circulation changes between 130 and 70 ka. *Geology* **1999**, *27*, 795–798. [CrossRef]
38. de Vernal, A.; Hillaire-Marcel, C.; Turon, J.-L.; Matthiessen, J. Reconstruction of sea-surface temperature, salinity, and sea-ice cover in the northern North Atlantic during the last glacial maximum based on dinocyst assemblages. *Can. J. Earth Sci.* **2000**, *37*, 725–750. [CrossRef]
39. Rashid, H.; Boyle, E.A. Mixed-layer deepening during Heinrich Events: A Multi-Planktonic Foraminiferal  $\delta^{18}\text{O}$  approach. *Science* **2007**, *318*, 439–441. [CrossRef]
40. Jonkers, L.; Moros, M.; Prins, M.A.; Dokken, T.; Dahl, C.A.; Dijkstra, N.; Perner, K.; Brummer, G.-J.A. A reconstruction of sea surface warming in the northern North Atlantic during MIS 3 ice-rafting events. *Quat. Sci. Rev.* **2010**, *29*, 1791–1800. [CrossRef]
41. Simstich, J.; Sarnthein, M.; Erlenkeuser, H. Paired  $d^{18}\text{O}$  signals of *Neogloboquadrina pachyderma* (s) and *Turborotalita quinqueloba* show thermal stratification structure in Nordic Seas. *Mar. Micropaleontol.* **2003**, *48*, 107–125. [CrossRef]
42. Wu, G.; Hillaire-Marcel, C. Oxygen isotope composition of sinistral *Neogloboquadrina pachyderma* tests in surface sediments: North Atlantic Ocean. *Geochim. Cosmochim.* **1994**, *58*, 1303–1312. [CrossRef]
43. Hodell, D.A.; Curtis, J.H. Oxygen and carbon isotopes of detrital carbonate in North Atlantic Heinrich Events. *Mar. Geol.* **2008**, *256*, 30–35. [CrossRef]
44. Stangeew, E. Distribution and Isotopic Composition of Living Planktonic Foraminifera *N. pachyderma* (sinistral) and *T. quinqueloba* in the High Latitude North Atlantic. Ph.D. Thesis, Christian-Albrechts Universität Kiel, Kiel, Germany, 2001; p. 91.
45. Stuiver, M.; Reimer, P.J.; Reimer, R.W. CALIB 8.2 [WWW Program]. 2021. Available online: <http://calib.org> (accessed on 21 February 2021).
46. Heaton, T.J.; Köhler, P.; Butzin, M.; Bard, E.; Reimer, R.W.; Austin, W.E.N.; Bronk Ramsey, C.; Grootes, P.M.; Hughen, K.A.; Kromer, B.; et al. Marine20-The Marine Radiocarbon Age Calibration Curve (0-55,000 cal BP). *Radiocarbon* **2020**, *62*, 779–820. [CrossRef]
47. Lisiecki, L.E.; Stern, J.V. Regional and global benthic  $\delta^{18}\text{O}$  stacks for the last glacial cycle. *Paleoceanography* **2016**, *31*, 1368–1394. [CrossRef]
48. Rashid, H.; MacKillop, K.; Sherwin, J.; Piper, D.J.W.; Marche, B.; Vermooten, M. Slope instability on a shallow contourite-dominated continental margin, southeastern Grand Banks, eastern Canada. *Mar. Geol.* **2017**, *393*, 203–215. [CrossRef]
49. McManus, J.F.; Bond, G.C.; Broecker, W.S.; Johnsen, S.; Labeyrie, L.; Higgins, S. High-resolution climate records from the N. Atlantic during the last interglacial. *Nature* **1994**, *371*, 326–329. [CrossRef]
50. Rahmstorf, S. Ocean circulation and climate during the past 120,000 years. *Nature* **2002**, *419*, 207–214. [CrossRef]
51. Holliday, N.P.; Bersch, M.; Berx, B.; Chafik, L.; Cunningham, S.A.; Florindo-López, C.; Hátún, H.; Johns, W.E.; Josey, S.A.; Larsen, K.; et al. Ocean circulation causes the largest freshening event for 120 years in eastern subpolar North Atlantic. *Nat. Commun.* **2020**, *11*, 1–15. [CrossRef]
52. Irvali, N.; Galaasen, E.V.; Ninnemann, U.S.; Rosenthal, Y.; Born, A.; Kleiven, F. A low climate threshold for south Greenland Ice Sheet demise during the Late Pleistocene. *Proc. Natl. Acad. Sci. USA* **2020**, *117*, 190–195. [CrossRef]
53. Galaasen, E.V.; Ninnemann, U.S.; Irvali, N.; Kleiven, H.F.; Rosenthal, Y.; Kissel, C.; Hodell, D.A. Rapid Reductions in North Atlantic Deep Water During the Peak of the Last Interglacial Period. *Science* **2014**, *343*, 1129–1132. [CrossRef]
54. Galaasen, E.V.; Ninnemann, U.S.; Kessler, A.; Irvali, N.; Rosenthal, Y.; Tjiputra, J.; Bouttes, N.; Roche, D.M.; Kleiven, H.F.; Hodell, D.A. Interglacial instability of North Atlantic Deep Water ventilation. *Science* **2020**, *367*, 1485–1489. [CrossRef]
55. Winsor, K.; Carlson, A.E.; Klinkhammer, G.P.; Stoner, J.S.; Hatfield, R.G. Evolution of the northeast Labrador Sea during the last interglaciation. *Geochem. Geophys. Geosyst.* **2012**, *13*, Q11006. [CrossRef]
56. Martinson, D.G.; Pisias, N.G.; Hays, J.D.; Imbrie, J.; Moore, T.C.; Shackleton, N.J. Age dating and the orbital theory of the ice ages: Development of a high-resolution 0 to 300,000-year chronostratigraphy. *Quat. Res.* **1987**, *27*, 1–29. [CrossRef]
57. Rashid, H.; Hesse, R.; Piper, D.J.W. Evidence for an additional Heinrich event between H5 and H6 in the Labrador Sea. *Paleoceanography* **2003**, *18*, 1077. [CrossRef]
58. Villanueva, J.; Grimalt, J.O.; Cortijo, E.; Vidal, L.; Labeyrie, L. Assessment of sea surface temperature variations in the central North Atlantic using the alkenone unsaturation index (Uk'37). *Geochim. Cosmochim. Acta* **1998**, *62*, 2421–2427. [CrossRef]

59. Govin, A.; Braconnot, P.; Capron, E.; Cortijo, E.; Duplessy, J.C.; Jansen, E.; Labeyrie, L.; Landais, A.; Marti, O.; Michel, E.; et al. Persistent influence of ice sheet melting on high northern latitude climate during the early Last Interglacial. *Clim. Past* **2012**, *8*, 3239–3286. [[CrossRef](#)]
60. Jullien, E.; Grousset, F.E.; Hemming, S.R.; Peck, V.L.; Hall, I.R.; Jeantet, C.; Billy, I. Contrasting conditions preceding MIS3 and MIS2 Heinrich events. *Glob. Planet. Chang.* **2006**, *54*, 225–238. [[CrossRef](#)]
61. Mao, L.-J.; Piper, D.J.W.; Saint-Ange, F.; Andrews, J.T. Labrador Current fluctuation during the last glacial cycle. *Mar. Geol.* **2018**, *395*, 234–246. [[CrossRef](#)]
62. Berger, A. Long-term variations of daily insolation and Quaternary climatic change. *J. Atmos. Sci.* **1978**, *35*, 2362–2367. [[CrossRef](#)]
63. Keigwin, L.D.; Lehman, S.J. Deep circulation change linked to HEINRICH event 1 and Younger Dryas in a middepth North Atlantic core. *Paleoceanography* **1994**, *9*, 185–194. [[CrossRef](#)]
64. Bond, G.C.; Lotti, R.R. Iceberg discharges into the North Atlantic on millennial time scales during the last glaciation. *Science* **1995**, *267*, 1005–1010. [[CrossRef](#)] [[PubMed](#)]
65. Chapman, D.C. Boundary layer control of buoyant coastal currents and the establishment of a shelf break point. *J. Physical Oceanography* **2000**, *30*, 2941–2955. [[CrossRef](#)]
66. Condron, A.; Winsor, P. Meltwater routing and the Younger Dryas. *Proc. Natl. Acad. Sci. USA* **2012**, *109*, 19928–19933. [[CrossRef](#)] [[PubMed](#)]
67. Bond, G.C.; Showers, W.; Cheseby, M.; Lotti, R.; Almasi, P.; deMenocal, P.; Priore, P.; Cullen, H.; Hajdas, I.; Bonani, G. Persistent solar influence on North Atlantic climate during the Holocene. *Science* **2001**, *294*, 2130–2136. [[CrossRef](#)]
68. Hoogakker, B.A.A.; McCave, I.N.; Elderfield, H.; Hillaire-Marcel, C.; Simstich, J. Holocene climate variability in the Labrador Sea. *J. Geol. Soc.* **2014**, *172*, 272–277. [[CrossRef](#)]